arXiv:1609.06607v1 [cond-mat.quant-gas] 21 Sep 2016

Creating spin-one fermions in the presence of artificial spin-orbit fields: Emergent spinor physics and spectroscopic properties

Doga Murat Kurkcuoglu and C. A. R. Sá de Melo
School of Physics, Georgia Institute of Technology, Atlanta, Georgia 30332, USA
(Dated: February 3, 2015)

We propose the creation and investigation of a system of spin-one fermions in the presence of artificial spin-orbit coupling, via the interaction of three hyperfine states of fermionic atoms to Raman laser fields. We explore the emergence of spinor physics in the Hamiltonian described by the interaction between light and atoms, and analyze spectroscopic properties such as dispersion relation, Fermi surfaces, spectral functions, spin-dependent momentum distributions and density of states. Connections to spin-one bosons and SU(3) systems is made, as well relations to the Lifshitz transition and Pomeranchuk instability are presented.

PACS numbers: 03.75.Ss, 67.85.Lm, 67.85.-d

The field of ultra-cold atoms has been a very prolific area of research with the experimental realization of several fundamental theoretical ideas such as Bose-Einstein condensation (BEC) [1, 2], the Mott-Insulator transition in the Bose-Hubbard model [3] and the evolution from BCS to BEC superfluidity [4–6]. Strong connections to standard condensed matter physics have been developed, specially in the case of optical lattices, and some very unique situations have also emerged due to the ability to control the trapping of atoms with different hyperfine states [7]. One of these special cases is the creation of spin-1/2 bosons, where only two internal or hyperfine states of bosonic atoms with integer spin were trapped and investigated experimentally [8, 9]. The existence of bosonic or fermionic atoms with large integer or half-integer spins which have interactions that are independent of the hyperfine states could lead to the realization of SU(N) invariant Hamiltonians, as evidenced experimentally in the case of Strontium (Sr) atoms [10]. The realization of such exotic situations is promoting the field of ultra-cold atoms beyond the stage of simulating known Hamiltonians from diverse areas of Physics to the stage of creating novel Hamiltonians, which have no direct counterpart in any area of Physics. An important example is the unusual case of spin-1/2 bosons in the presence of artificial spin-orbit coupling, which was created experimentally [11, 12] and its effects on Bose-Einstein condensation were studied thoroughly [13–16].

In this manuscript, we propose also another exotic case corresponding to the creation of spin-one fermions in the presence of artificial spin-orbit coupling, instead of the traditional spin-1/2 fermion case that has been recently studied theoretically [17–21] and experimentally [22–25]. A potential candidate for such a situation is the Fermi isotope of Potassium (^{40}K), which possess several hyperfine states that can be trapped. However, other high spin Fermi atoms are also potential candidates, such as Ytterbium (Yt) or Strontium (Sr). We envision a situation that only three hyperfine states of the Fermi atom are trapped, and assume that Raman beams are used to produce artificial spin-orbit coupling in the fermionic system via light-atom interactions. The possibility of trapping three hyperfine states of fermions has a direct connection to color superconductivity, as we can also view the three different hyperfine states as different colors (red, green and blue), and by controlling the interactions between atoms in different hyperfine states we could create several types of paired states, such as, red-green, red-blue, and green-blue [26]. We can also relate this system to multi-band materials by thinking of the hyperfine states as labelling different energy bands, and if interactions can be tunned to produce superfluidity, we can create a multi-band superfluid in the presence of spin-orbit coupling. Thus, the creation of spin-one fermions is not in violation of the spin-statistics theorem [27], as the spin degrees of freedom truly correspond to pseudo-spin states (color or band index). However, such a system possesses interesting spinor physics and spectroscopic properties to be discussed next.

We consider fermionic atoms with three hyperfine states coupled via Raman processes between states 1 and 2 as well as 2 and 3, such that there is a net momentum transfer $\mathbf{Q}_{12}$ to state 1 and $-\mathbf{Q}_{23}$ to state 3, resulting in the light-atom Hamiltonian matrix

$$\mathbf{H}_{\rm LA}(\mathbf{k}) = \begin{pmatrix} \varepsilon_1(\mathbf{k}) & \Omega_{12} & 0 \\ \Omega_{12}^* & \varepsilon_2(\mathbf{k}) & \Omega_{23} \\ 0 & \Omega_{23}^* & \varepsilon_3(\mathbf{k}) \end{pmatrix}, \qquad (1)$$

written in the rotating frame, where the ℓ^{th} state carries momentum $\mathbf{k}-\mathbf{k}_\ell$. Each diagonal element $\varepsilon_\ell(\mathbf{k}) = (\mathbf{k}-\mathbf{k}_\ell)^2/(2m) + \eta_\ell$ is the sum of the kinetic energy $(\mathbf{k}-\mathbf{k}_\ell)^2/(2m)$ of the ℓ^{th} hyperfine state after the net momentum transfer $\mathbf{k}_\ell$ and internal energy η_ℓ. The momenta $\mathbf{k}_\ell$ are $\mathbf{k}_1 = \mathbf{Q}_{12}$, $\mathbf{k}_2 = \mathbf{0}$ and $\mathbf{k}_3 = -\mathbf{Q}_{23}$. The terms $\Omega_{\ell m}$ are the Rabi frequencies coupling of adjacent hyperfine states, which can be taken to be real such that $\Omega_{12} = \Omega_{12}^*$ and $\Omega_{23} = \Omega_{23}^*$. We can define an energy reference via the sum $\sum_\ell \eta_\ell = \eta$, in this case we can set $\eta_1 = -\delta$, $\eta_2 = \eta$ and $\eta_3 = +\delta$.

When the Raman beams form an arbitrary angle, mo-

mentum transfers can be chosen to be $\mathbf{k}_1 = k_T\hat{\mathbf{x}}$, $\mathbf{k}_2 = \mathbf{0}$, and $\mathbf{k}_3 = -k_T\hat{\mathbf{x}}$, with $0 \leq k_T \leq 2k_R$, where $k_R = 2\pi/\lambda$ is the recoil momentum, and λ is the photon wavelength. Assuming that all Rabi frequencies are the same ($\Omega_{12} = \Omega_{23} = \Omega$) the Hamiltonian of Eq. (1) reduces to

$$\begin{pmatrix} \varepsilon_0(\mathbf{k}) - h_z(\mathbf{k}) + b_z & -h_x/\sqrt{2} & 0 \\ -h_x/\sqrt{2} & \varepsilon_0(\mathbf{k}) & -h_x/\sqrt{2} \\ 0 & -h_x/\sqrt{2} & \varepsilon_0(\mathbf{k}) + h_z(\mathbf{k}) + b_z \end{pmatrix}, \tag{2}$$

where $\varepsilon_0(\mathbf{k}) = \mathbf{k}^2/(2m) + \eta$ is a reference kinetic energy which is the same for all hyperfine states, $h_z(\mathbf{k}) = 2k_Tk_x/(2m) + \delta$ is a momentum dependent Zeeman field along the z-direction, which is transverse to the momentum transfer direction, $h_x(\mathbf{k}) = -\sqrt{2}\Omega$ is the *spin-flip* (Rabi) field, and $b_z = k_T^2/(2m) - \eta$ is the quadratic Zeeman term. A similar Hamiltonian was created recently in the NIST group for spin-one bosonic atoms [28].

The light-atom Hamiltonian matrix displayed in Eq. (2) can be expanded in terms of a subset of the SU(3) Gell-Mann matrices that includes the identity $\mathbf{1}$ and the spin-one angular momentum matrices $\mathbf{J}_x$, $\mathbf{J}_z$ and $\mathbf{J}_z^2$. In compact notation, the expansion reads

$$\mathbf{H}_{\rm LA}(\mathbf{k}) = \varepsilon_0(\mathbf{k})\mathbf{1} - h_x(\mathbf{k})\mathbf{J}_x - h_z(\mathbf{k})\mathbf{J}_z + b_z\mathbf{J}_z^2. \tag{3}$$

Written in this form the light-atom Hamiltonian matrix can be interpreted as describing spin-one fermions in the presence of momentum dependent *magnetic* field components $h_x(\mathbf{k})$, $h_z(\mathbf{k})$ and a quadratic Zeeman shift parametrized by the coefficient b_z. Notice that when $b_z = 0$ the system reduces to a spin-one fermion in the presence of a momentum dependent magnetic field. In this case the eigenvalues are $E_\alpha(\mathbf{k}) = \varepsilon_0(\mathbf{k}) - m_\alpha|h_{\rm eff}(\mathbf{k})|$, with $m_\alpha = \{+1, 0, -1\}$, where the effective momentum dependent magnetic field amplitude is $|h_{\rm eff}(\mathbf{k})| = \sqrt{|h_x(\mathbf{k})|^2 + |h_z(\mathbf{k})|^2}$.

Using Cardano's method [29], the eigenvalues of this spin-one fermion Hamiltonian can be obtained analytically from the zeros of the characteristic polynomial $P(\omega) = \det\left[\omega\mathbf{1} - \mathbf{H}_{\rm LA}(\mathbf{k})\right]$, but the general expressions are quite cumbersone. Thus, we also obtain the eigenvalues $E_\alpha(\mathbf{k})$ by direct diagonalization of $\mathbf{H}_{\rm LA}(\mathbf{k})$ to validate the analytical results and order them such that $E_1(\mathbf{k}) > E_2(\mathbf{k}) > E_3(\mathbf{k})$.

In Fig. 1, we show plots of eigenvalues $E_\alpha(\mathbf{k})$ in qualitatively different situations corresponding to momentum transfer $k_T = 0.5k_R$, Rabi frequency $\Omega = 0.35E_R$ and three different values of the quadratic Zeeman shift $b_z = \{-E_R, 0, E_R\}$. Along the k_x direction, notice that a double minimum is present in $E_3(\mathbf{k})$ when $b_z < 0$, and that a double minimum appears in $E_2(\mathbf{k})$, when $b_z > 0$, while $E_3(\mathbf{k})$ is very flat near $k_x = 0$ and $E_2(\mathbf{k})$ has a single minimum when $b_z = 0$. If our system consisted of spin-one bosonic atoms, a phase transition would take place between a BEC at finite and zero momentum as b_z is increased from negative to positive values.

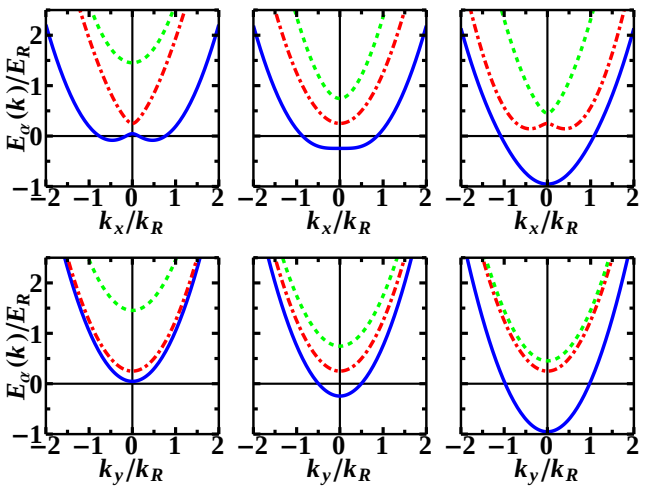

FIG. 1. (color online) Eigenvalues $E_\alpha(\mathbf{k})$ in qualitatively different situations corresponding to momentum transfer $k_T = 0.5k_R$, Rabi frequency $\Omega = 0.35E_R$ and quadratic Zeeman shift $b_z = -E_R$ (left); $b_z = 0$ (middle); $b_z = E_R$ (right). The dashed-green line corresponds to $E_1(\mathbf{k})$, the dot-dashed-red line to $E_2(\mathbf{k})$, and the solid blue to $E_3(\mathbf{k})$. The top and bottom panels corresponds to cuts along the $(k_x, 0, 0)$ and $(0, k_y, 0)$ directions, respectively.

Since we are dealing with spin-one fermions, we investigate next the Fermi surfaces that emerge due to light-atom interactions as a function of the control parameters k_T, Ω and b_z, and make connections to Lifshitz and Pomeranchuk instabilities found in condensed matter physics. We define an effective Fermi momentum k_F via the total particle density $n = 3k_F^3/(6\pi^2)$, where the factor of 3 indicates the presence of three internal states which lead to the three bands of the many-fermion system. We also define the effective Fermi energy as $E_F = k_F^2/(2m)$ and make plots of Fermi surfaces are made assuming a density of $n = 10^{14}$atoms/cm^3.

In Fig. 2, we illustrate qualitatively different situations corresponding to $k_T = 0.5k_R$, $\Omega = 0.35E_R$ and $b_z = \{-E_R, 0, E_R\}$. Notice that in the middle panel of Fig. 2 there is no quadratic Zeeman shift ($b_z = 0$), but k_T and Ω are non-zero. As described above, this implies that new fermionic bands $E_\alpha(\mathbf{k}) = \varepsilon_0(\mathbf{k}) - m_\alpha|h_{\rm eff}(\mathbf{k})|$, with $m_\alpha = \{+1, 0, -1\}$, emerge from three degenerate bands $\varepsilon_0(\mathbf{k})$. As a result, identical spherical Fermi surfaces associated with $\varepsilon_0(\mathbf{k})$ become non-degenerate since the new energy dispersions are controlled by $|h_{\rm eff}(\mathbf{k})|$, which is a function of k_T and Ω. With the exception of the central band $E_2(\mathbf{k})$, which still produces a spherical Fermi surface, the other two bands possess anisotropic Fermi surfaces due to $|h_{\rm eff}(\mathbf{k})|$.

These effects are reminiscent of the Pomeranchuk [30] instability in condensed matter physics, where deforma-

tions in Fermi surfaces may emerge spontaneously in systems with anisotropic density-density interactions, without violating Luttinger's theorem [31]. In such cases, the resulting interactions produce deformations in the Fermi surfaces of the system, making them incompatible with the underlying symmetry of the crystal. The easiest way to see this connection is to analyze the toy Hamiltonian

$$H=\sum_{\mathbf{k},\alpha}\left[\varepsilon(\mathbf{k})\hat{n}_{\alpha}(\mathbf{k})\right]+\frac{1}{2}\sum_{\mathbf{k},\mathbf{k}'\alpha\beta}F_{\alpha\beta}(\mathbf{k},\mathbf{k}')\hat{n}_{\alpha}(\mathbf{k})\hat{n}_{\beta}(\mathbf{k}')$$

where $\hat{n}_{\alpha}(\mathbf{k})=c_{\alpha}^{\dagger}(\mathbf{k})c_{\alpha}(\mathbf{k})$ is the number operator for spin α. The replacement of $\hat{n}_{\alpha}(\mathbf{k})=\langle\hat{n}_{\alpha}(\mathbf{k})\rangle+\delta\hat{n}_{\alpha}(\mathbf{k}$ leads to the mean-field Hamiltonian $H=\sum_{\mathbf{k},\alpha}\left[E_{\alpha}(\mathbf{k})\hat{n}_{\alpha}(\mathbf{k})\right]+C$. The energy for internal state α is $E_{\alpha}(\mathbf{k})=\varepsilon(\mathbf{k})-h_{\alpha}(\mathbf{k})$. where $\varepsilon(\mathbf{k})=\mathbf{k}^{2}/(2m)$, is the kinetic energy of fermions of mass m, and $h_{\alpha}(\mathbf{k})=-\sum_{\beta,\mathbf{k}'}\left[F_{\alpha\beta}(\mathbf{k},\mathbf{k}')+F_{\beta\alpha}(\mathbf{k}',\mathbf{k})\right]\langle\hat{n}_{\beta}(\mathbf{k}')\rangle$, is the *effective* field affecting the α-band. Lastly, the constant energy reference is $C=\frac{1}{2}\sum_{\mathbf{k},\mathbf{k}'\alpha\beta}F_{\alpha\beta}(\mathbf{k},\mathbf{k}')\langle\hat{n}_{\alpha}(\mathbf{k})\rangle\langle\hat{n}_{\beta}(\mathbf{k}')\rangle$. Notice that when $h_{\alpha}(\mathbf{k})$ does not have spherical symmetry, then the Fermi surface for state α is deformed.

In Fig. 2, a clear signature of the Pomeranchuk-like instability can be seen for the band with energy $E_2(\mathbf{k})$ shown as the red dot-dashed line. However, notice that for fixed k_T and Ω, what drives the Fermi surface deformations is the quadratic Zeeman coupling b_z, that is, the J_z-J_z spinor coupling instead of the density-density interactions. When $b_z=0$, the Fermi surface corresponding to $E_2(\mathbf{k})$ is spherically symmetric, however when $b_z>0$ ($b_z<0$) this Fermi surface suffers a predominant deformation along the k_x (k_y) direction. The Ising-Nematic order parameter $\mathcal{N}_2=\int d\mathbf{k}\left[k_y^2+k_z^2-2k_x^2\right]\langle\phi_2^{\dagger}(\mathbf{k})\phi_2(\mathbf{k})\rangle$ becomes zero for $b_z=0$, positive for $b_z<0$ and negative for $b_z>0$, where $\phi_2^{\dagger}(\mathbf{k})$ is the creation operator for eingestate 2. Similar Pomeranchuk-type deformations occur for $E_1(\mathbf{k})$ or $E_3(\mathbf{k})$, however deformations are already present even for $b_z=0$, because the spin-orbit coupling contains non-spherically-symmetric contributions through the effective field $h_{\rm eff}(\mathbf{k})$.

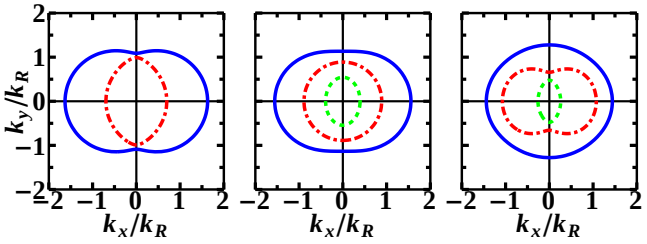

FIG. 2. (color online) Fermi surfaces are shown in qualitatively different situations corresponding to momentum transfer $k_T=0.5k_R$, Rabi frequency $\Omega=0.35E_R$ and three different values of the quadratic Zeeman shift $b_z=-E_R$ (left); (b) $b_z=0$ (middle); (c) $b_z=E_R$ (right). The values of the chemical potential are $\mu=1.23E_R$ (left), $\mu=1.04E_R$ (middle), $\mu=0.68E_R$ (right) for particle density $n=10^{14}$atoms/cm^3.

We also mention in passing the existence of a Lifshitz transition [32], which for fixed momentum transfer $\mathbf{k}_T$ and particle density n, can be tuned via the Rabi frequency Ω and the quadratic Zeeman coupling b_z. In Fig. 2, one can see a Lifsthitz transition for fixed Ω and changing b_z, as three Fermi surfaces (genus 3) for $b_z=0$ are reduced to two Fermi surfaces (genus 2) for $b_z=-E_R$. A phase diagram can be constructed mapping out these topological changes in the Ω versus b_z plane.

The effects of artificial spin-orbit and quadratic Zeeman coupling, due to light-atom interactions via the Raman scheme, can be further explored by investigating the three-component spinor wavefunctions. For this purpose, we write the Hamiltonian as

$$H_{\rm LA}=\sum_{\mathbf{k}}\mathbf{\Psi}_{\mathbf{k}}^{\dagger}\mathbf{H}_{\rm LA}(\mathbf{k})\mathbf{\Psi}_{\mathbf{k}},\tag{4}$$

where $\mathbf{\Psi}_{\mathbf{k}}$ is a three-component spinor with $\mathbf{\Psi}_{\mathbf{k}}^{\dagger}=\left(\psi_1^{\dagger}(\mathbf{k}),\psi_2^{\dagger}(\mathbf{k}),\psi_3^{\dagger}(\mathbf{k})\right)$, where $\psi_s^{\dagger}(\mathbf{k})$ represents the creation of a fermion in spin state s. When $s=1$, the atom has momentum $\mathbf{k}-\mathbf{k}_T$ and $m_1=+1$; when $s=2$, the atom has momentum $\mathbf{k}$ and $m_2=0$; and when $s=3$, the atom has momentum $\mathbf{k}+\mathbf{k}_T$ and $m_3=-1$.

The Hamiltonian $H_{\rm LA}$ can be diagonalized via the rotation $\mathbf{\Phi}(\mathbf{k})=\mathbf{U}(\mathbf{k})\mathbf{\Psi}(\mathbf{k})$, which connects the three-component spinor $\mathbf{\Psi}(\mathbf{k})$ in the original spin basis to the three-component spinor $\mathbf{\Phi}(\mathbf{k})$ representing the basis of eigenstates. The matrix $\mathbf{U}(\mathbf{k})$ is unitary and satisfies the relation $\mathbf{U}^{\dagger}(\mathbf{k})\mathbf{U}(\mathbf{k})=\mathbf{1}$. The diagonalized Hamiltonian is $\mathbf{H}_D(\mathbf{k})=\mathbf{U}(\mathbf{k})\mathbf{H}_{\rm LA}\mathbf{U}^{\dagger}(\mathbf{k})$ with matrix elements $\left[\mathbf{H}_D(\mathbf{k})\right]_{\alpha\beta}=E_{\alpha}(\mathbf{k})\delta_{\alpha\beta}$, where $E_{\alpha}(\mathbf{k})$ are the eigenvalues of $\mathbf{H}_{\rm LA}(\mathbf{k})$ discussed above. The three-component spinor in the eigenbasis is $\mathbf{\Phi}^{\dagger}(\mathbf{k})=\left(\phi_1^{\dagger}(\mathbf{k}),\phi_2^{\dagger}(\mathbf{k}),\phi_3^{\dagger}(\mathbf{k}),\right)$, where $\phi_{\alpha}^{\dagger}(\mathbf{k})$ is the creation operator of a fermion with eigenenergy $E_{\alpha}(\mathbf{k})$. The unitary matrix

$$\mathbf{U}(\mathbf{k})=\begin{pmatrix}u_{11}(\mathbf{k}) & u_{12}(\mathbf{k}) & u_{13}(\mathbf{k})\\ u_{21}(\mathbf{k}) & u_{22}(\mathbf{k}) & u_{23}(\mathbf{k})\\ u_{31}(\mathbf{k}) & u_{32}(\mathbf{k}) & u_{33}(\mathbf{k})\end{pmatrix}\tag{5}$$

has rows that satisfy the normalization condition $\sum_s|u_{\alpha s}(\mathbf{k})|^2=1$.

Using a Stern-Gerlach technique, another spectroscopic property that can be measured is the spin-dependent momentum distribution

$$n_s(\mathbf{k})=\sum_{\alpha}|u_{\alpha s}(\mathbf{k})|^2f[E_{\alpha}(\mathbf{k})].\tag{6}$$

We can fix the average number of particles $N_s=\sum_{\mathbf{k}}n_s(\mathbf{k})$ in each state s independently, in which case chemical potentials μ_s for each state s are necessary. However, when the total average number of particles $N=\sum_s N_s=\sum_{s,\alpha}|u_{\alpha s}(\mathbf{k})|^2f[E_{\alpha}(\mathbf{k})]$ is fixed, we need only

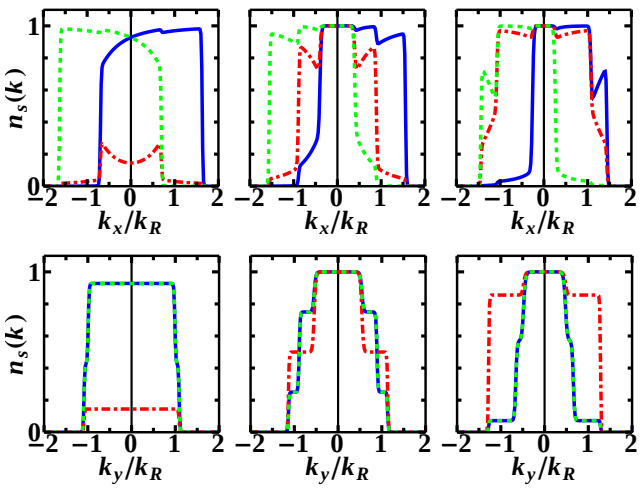

FIG. 3. (color online) Momentum distributions $n_s(\mathbf{k})$ for $s = 1$ ($m_1 = +1$) (blue-solid curves), $s = 2$ ($m_2 = 0$) (red-dot-dashed curves) and $s = 3$ ($m_3 = -1$) (green-dashed curves), with $T = 0.02E_R \approx 0.01E_F$. The parameter values are $b_z = -E_R$ (left panels), $b_z = 0$ (middle panels) and $b_z = +E_R$ (right panels), with $k_T = 0.5k_R$ and $\Omega = 0.35E_R$.

one chemical potential μ. The use of the normalization condition $\sum_s |u_{\alpha s}(\mathbf{k})|^2 = 1$ leads to $N = \sum_\alpha f[E_\alpha(\mathbf{k})]$.

In Fig. 3, we show $n_s(\mathbf{k})$ at low temperatures for the simpler case where there is only one chemical potential. The cross sections along k_x with $k_y = k_z = 0$ are shown in Fig. 3 top panels, while the cross sections along k_y with $k_x = k_z = 0$ are shown in Fig. 3 lower panels. In the top panels of Fig. 3, notice that $n_s(\mathbf{k})$ for states $s = 1$ ($m_1 = +1$) and $s = 3$ ($m_3 = -1$) do not have well defined parity, but are mirror images of each other. This is a reflection of the Hamiltonian invariance under the transformation $(k_x, m_1) \to (-k_x, m_3)$ and $(k_x, m_3) \to (-k_x, m_1)$.

The momentum distributions shown in Fig. 3 can be understood as follows. The momentum transfer along the k_x direction shifts the center of mass of the atom in state $s = 1$ with $m_1 = +1$ ($s = 3$ with $m_3 = -1$) to be around k_T ($-k_T$). While there is no momentum shift for the state $s = 2$ with $m_2 = 0$. In the limit of $\Omega \to 0$, $n_s(\mathbf{k})$ along k_x have square shapes characteristic of degenerate fermions for each of the spin states. However, momentum transfer can only occur when the lasers are on, which means $\Omega \neq 0$. This leads to mixing of the spin states and to a modification of the trivial momentum distributions via the coherence factors $|u_{\alpha s}(\mathbf{k})|^2$. The dramatic effects of the coherence factors is seen on Fig. 3 (top panels) where finite Ω causes strong deviations from square momentum distributions, due to the momentum-dependent mixing of different spin states. However, $n_s(\mathbf{k})$ along the k_y direction experience no momentum transfer and are centered around zero. For $k_x = 0$, the light-atom Hamiltonian matrix is invariant under the transformations $(k_y, m_s) \to (-k_y, m_s)$, $(k_y, m_1) \to (-k_y, m_3)$, and $(k_y, m_3) \to (-k_y, m_1)$, such that the corresponding $n_s(\mathbf{k})$ along k_y for states $s = 1$ and $s = 3$ are identical. The square like structures that emerge are a consequence of the less dramatic dependence of the coherence factors $|u_{\alpha s}(\mathbf{k})|^2$ on k_y. By symmetry, the same square structures also appear along the k_z direction.

Notice that as b_z increases from negative to positive (left to right panels in Fig. 3), $n_s(\mathbf{k})$ for state $s = 2$ along the k_x and k_y directions increase on average at fixed Ω. This enhancement occurs because the energy of the $s = 2$ state becomes increasingly lowered in comparison to the energy of the $s = 1, 3$ states, and spectral weight is transferred from states $s = 1, 3$ to $s = 2$, causing a corresponding decrease in the average $n_s(\mathbf{k})$ of the former states. When b_z becomes large and negative, the central state ($s = 2$) is pushed up in energy with respect to the $s = 1, 3$ states, and for densities such that the Fermi energy crosses only the two lowest states ($s = 1, 3$), the system reduces to effective spin-1/2 fermions. However, when b_z becomes large and positive, the central state ($s = 2$) is pushed down in energy with respect to the $s = 1, 3$ states, and for densities such that the Fermi energy only crosses the $s = 2$ state, the system reduces to effective spin-zero (spinless) fermions.

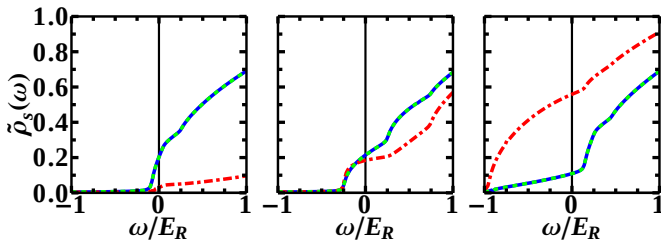

FIG. 4. (color online) Density of states $\widetilde{\rho}_s(\omega) = \rho_s(\omega)E_F/N$ for $s = 1$ ($m_1 = +1$) (blue-solid lines), $s = 2$ ($m_2 = 0$) (red-dot-dashed lines), and $s = 3$ ($m_3 = -1$) (green-dashed lines). N is the total number of particles and E_F is the effective Fermi energy. We use a line-width broadening $\delta_{\ell w} = 0.01E_R$. The parameters used are $b_z = -E_R$ (left panel), $b_z = 0$ (middle panel) and $b_z = +E_R$ (right panel), with $k_T = 0.5k_R$ and $\Omega = 0.35E_R$ and $E_F = 1.95E_R$.

The last spectroscopic quantity that we analyze is the spin-dependent density of states (DOS)

$$\rho_s(\omega) = \sum_{\mathbf{k},\alpha} |u_{\alpha s}(\mathbf{k})|^2 \delta(\omega - E_\alpha(\mathbf{k})). \tag{7}$$

Below the minimum of $E_3(\mathbf{k})$ there are no states available, that is, $\rho_s(\omega) = 0$ for $\omega \leq \omega_*(\Omega, b_z, k_T) = \min_{\mathbf{k}} E_3(\mathbf{k})$. The spin-dependent DOS for $\Omega = 0.35E_R$ and $b_z = \{-E_R, 0, E_R\}$ are shown in Fig. 4. Notice that for $b_z = -E_R$ (left panel) the spin-dependent DOS is non-zero only when $\omega \geq -0.09E_R$ and that for small values of $\gamma = (\omega - \omega_*)/E_R$, the main contributions to the total DOS $\rho(\omega) = \sum_s \rho_s(\omega)$ come from states $s = 1, 3$. In addition, for $b_z = 0$ (central panel), $\rho_s(\omega) \geq 0$ when

$\omega \geq -0.27E_R$, and the DOS for each spin component are comparable for small values of γ. However, for $b_z = +E_R$ (right panel), $\rho_s(\omega) \geq 0$ when $\omega \geq -1.00E_R$, and the main contribution to $\rho(\omega)$ comes from $\rho_2(\omega)$ for small values of γ, as state $s = 2$ has the lowest energy.

In conclusion, we have proposed the creation of spin-one fermions in the presence of spin-orbit fields and quadratic Zeeman shifts induced by light-atom interactions using a Raman coupling scheme. By adjusting the quadratic Zeeman shift, we have shown that we can tune the system from spin-zero to spin-one to spin-1/2 fermions. We have analyzed Lifshitz and Pomeranchuk instabilities for varying quadratic Zeeman shifts and studied several spectroscopic properties including energy dispersion, Fermi surfaces, spectral function, spin-dependent momentum distribution and density of states.

[1] S. N. Bose, Z. Phys. **26**, 178 (1924).
[2] A. Einstein, Preuss. Akad. Wiss. Berlin Ber. **22**, 261 (1924).
[3] Matthew P. A. Fisher, Peter B. Weichman, G. Grinstein, and Daniel S. Fisher, Phys. Rev. B **40**, 546 1989.
[4] A. J. Leggett, J. Phys. Colloq. **41**, 7 (1980).
[5] P. Nozières and S. Schmitt-Rink J. Low Temp. Phys. **59**, 195 (1985).
[6] C. A. R. Sá de Melo, M. Randeria, J. R. Engelbrecht, Phys. Rev. Lett. **71**, 3202 (1993).
[7] I. Bloch, J. Dalibard and W. Zwerger, Rev. Mod. Phys. **80**, 885 (2008).
[8] C. J. Myatt, E. A. Burt, R. W. Ghrist, E. A. Cornell, and C. E. Wieman, Phys. Rev. Lett. **78**, 586 (1997).
[9] Ismardo J. Bonalde, Thilo M. Brill, Weijun Yao,Boudewijn J. Verhaar and Isaac F. Silvera, J. Low Temp. Phys. **113**, 211 (1998).
[10] X. Zhang, M. Bishof, S. L. Bromley, C. V. Kraus, M. S. Safronova, P. Zoller, A. M. Rey, and J. Ye, Science **345**, 1467 (2014).
[11] Y. J. Lin, K. Jimenez-Garcia, and I. B. Spielman, Nature (London) **471**, 83 (2011).
[12] Jin-Yi Zhang, Si-Cong Ji, Zhu Chen, Long Zhang, Zhi-Dong Du, Bo, Yan, Ge-Sheng Pan, Bo Zhao, You-Jin Deng, Hui Zhai, Shuai Chen, and Jian-Wei Pan, Phys. Rev. Lett. **109**, 115301 (2012).
[13] Tin-Lun Ho and Shizhong Zhang Phys. Rev. Lett. **107**, 150403 (2011).
[14] Yun Li, Lev P. Pitaevskii, and Sandro Stringari, Phys. Rev. Lett. **108**, 225301 (2012).
[15] Tomoki Ozawa and Gordon Baym, Phys. Rev. Lett. **110**, 085304 (2013).
[16] Si-Cong Ji, Jin-Yi Zhang, Long Zhang, Zhi-Dong Du, Wei Zheng, You-Jin Deng, Hui Zhai, Shuai Chen, and Jian-Wei Pan, Nature Physics **10**, 314 (2014).
[17] M. Gong, S. Tewari, and C. Zhang, Phys. Rev. Lett. **107**, 195303 (2011).
[18] Z.-Q. Yu, and H. Zhai, Phys. Rev. Lett. **107**, 195305 (2011).
[19] H. Hu, L. Jiang, X.-J. Liu, and H. Pu, Phys. Rev. Lett. **107**, 195304 (2011).
[20] L. Han and C. A. R. Sá de Melo, Phys. Rev. A **85**, 011606(R) (2012)
[21] K. Seo, L. Han, C. A. R. Sá de Melo, Phys. Rev. Lett. **109**, 105303 (2012).
[22] P. Wang, Z. Q. Yu, Z. Fu, J. Miao, L. Huang, S. Chai, H. Zhai, and J. Zhang, Phys. Rev. Lett. **109**, 095301 (2012).
[23] L.W. Cheuk, A. T. Sommer, Z. Hadzibabic, T. Yefsah, W. S. Bakr, and M. W. Zwierlein, Phys. Rev. Lett. **109**, 095302 (2012).
[24] R. A. Williams, M. C. Beeler, L. J. LeBlanc, K. Jimnez-Garca, and I. B. Spielman, Phys. Rev. Lett. **111**, 095301 (2013).
[25] Zhengkun Fu, Lianghui Huang, Zengming Meng, Pengjun Wang, Long Zhang, Shizhong Zhang, Hui Zhai, Peng Zhang and Jing Zhang, Nature Physics **10**, 110 (2014).
[26] C. A. R. Sá de Melo, Physics Today **61**, October issue, 45 (2008).
[27] W. Pauli, Phys. Rev. **58**, 716 (1940).
[28] Ian Spielman, private communication.
[29] G. Cardano, *The Rules of Algebra (Ars Magna)* Dover, (2007).
[30] I. Ia. Pomeranchuk, Zh. Eskp. Teor. Fiz.**35**, 524 (1958).
[31] J. M. Luttinger, Physical Review **119** 1153, (1960).
[32] I. M. Lifshitz, Zh. Eksp. Teor. Fiz. **38**, 1569 (1960).

ABR1073 - Creating spin-one fermions in the presence of artificial spin-orbit fields: Emergent spinor physics and spectroscopic properties

Status:	With author(s)
Journal:	Physical Review A
Article type:	Rapid Communication
Section:	Atomic and molecular processes in external fields, including interactions with strong fields and short pulses
Received:	04Feb2015
Author(s):	Doga Murat Kurkcuoglu and C. A. R. S{\'a} de Melo
Corresponding Author:	Kurkcuoglu,Doga Murat <dogakurkcuoglu@gmail.com>
PACS:	03.75.Ss 67.85.Lm
Copyright/Right to Publish:	Received

Download Manuscript PDF (187 KB)